Nuclear Instruments and Methods in Physics Research A237 (1985) 225–233
North-Holland, Amsterdam

INVESTIGATION OF NONRELATIVISTIC ELECTRON BEAM TRAPPING IN A COMPTON SCATTERING FREE ELECTRON LASER SCHEME *

A. GOVER, S. RUSCHIN, R. OLSHAN, H. KLEINMAN, A. FRIEDMAN and B. STEINBERG

Faculty of Engineering, Tel-Aviv University, Ramat Aviv 69978, Israel

We describe the progress in an experimental project aimed towards basic studies of electron trapping effects and efficiency enhancement schemes in free electron lasers. The experimental scheme is based on two TEA CO_2 laser beams at different vibrational lines (wavelengths), a nonrelativistic (kV) electron beam and an accelerating field. The present minimum trapping efficiency detection capability of the system is 1–3%. The expected trapping under present conditions is close to this level, and will far surpass with further improvements.

1. Introduction

In an FEL, the free electrons which propagate in a transverse electric or magnetic wiggler field can give rise to amplification of the electro-magnetic wave by the process of stimulated Compton scattering [3–5], or magnetic bremsstrahlung [6–14]. This radiative process is saturated when the electrons are trapped in a "ponderomotive potential" wave [15,16] produced by the pump (wiggler) and signal fields.

Many suggestions have been made to increase the efficiency of free electron lasers by tapering the period or amplitude of the periodic magnetic field (wiggler) from the point where the electrons get trapped in the ponderomotive potential. The tapering slows down the phase velocity of the ponderomotive potential, causing the trapped electrons to slow down and release their kinetic energy by radiation [17–23]. Efficiency can also be enhanced by applying a moderate axial electric field to the trapped electrons, causing them to radiate energy [24,25].

Much advanced theoretical research has been conducted recently on the gain enhancement concepts previously mentioned. However, little experimental work was carried out to probe these schemes, their limitations, the degree of trapping and the mechanisms of detrapping in the presence and in the absence of an axial electric field or a tapered wiggler. In the light of the large amount of interest in high power, high efficiency FELs, the amount of experimental research presently being carried out in the nonlinear (saturation) regime utilizing these concepts is quite small. Hence, an experiment which could probe these theoretical concepts and their limitations would help in feasibility studies and in the continual development of full-scale free electron laser experiments of this kind.

To this end, an experiment for studying electron trapping effects and measuring electron trapping efficiency in a stimulated Compton scattering configuration is in progress in Tel-Aviv University. The experiment is based on two high-power TEA CO_2 laser beams operating at two different CO_2 vibrational lines, one serving as a pump wave and the other as a signal wave. The electron beam is synchronized with the pondermotive wave and since the difference in laser frequencies is small, the e-beam can be nonrelativistic. The aim of the experiment is the basic study of FEL interaction in the nonlinear regime, particularly with reference to efficiency enhanced FEL (using wiggler tapering or axial electric field) and electromagnetic pump FELs (two stage FEL). The experiment stimulates a conventional FEL experiment as viewed from a relativistic frame reference moving nearly at the e-beam velocity. For example, our experiment $\lambda_w \simeq 10\ \mu m \simeq \lambda_s$ is equivalent to a conventional static wiggler FEL experiment with $\lambda_w = 1$ cm, $\lambda_s = 500\ \mu m$ and $\gamma_z = 100$.

In the proposed experimental setup, stimulated emission of infrared radiation and optical gain are expected to take place. The optical gain effect due to the interaction of the laser beam and electrons is expected to be considerably less than the effect on the electron beam energy distribution; hence, only an analysis of the electron beam energy after the interaction will be performed. The results of the energy analysis will provide useful information on nonlinear characteristics of free electron laser interaction, trapping efficiency, and feasibility of efficiency enhancement schemes, such as wiggler tapering and axial field application.

The construction of the optical and electron-optical systems for the moderate energy resolution experimen-

* Research supported in parts by the Airforce Office of Scientific Research Grant AFOSR 82-0239.

0168-9002/85/$03.30

tal setup has recently been completed. Detection of the trapping effect is presently being pursued, along with further development and improvement of the data acquisition system.

The experiment concept is based on the expectation that during the 150 ns laser pulse, a fraction of the electron beam current will be trapped by the ponderomotive potential produced by the two laser beams inside the interaction region. These trapped electrons maintain a constant velocity, while the untrapped electrons are accelerated (or decelerated) by the axial electric field of a coil, which guides the electron beam. The trapped and untrapped electron species, arriving at different energies after the interaction region, are temporally separated in a low energy (20 eV) long drift region. The energy spectrum measurement is based on the "time of flight" technique.

2. Theoretical analysis

The investigated system is composed of two counter propagating high power optical beams and an electron beam (fig. 1). The wiggler and signal wave frequencies ω_w, ω_s are related by the Doppler shift formula

$$\omega_s = \frac{1+\beta_{0z}}{1-\beta_{0z}}\omega_w = (1+\beta_{0z})^2\gamma_{0z}^2\omega_w, \tag{1}$$

where $\gamma_{0z} = (1-\beta_{0z}^2)^{-1/2}$, $B_{0z} = V_{0z}/c$ and V_{0z} is the e-beam axial velocity. The power in one of the optical beams can grow by stimulated emission on account of the power in the other optical beam and the electron beam power.

In the moving frame a static wiggler magnetic field looks like an incoming real electromagnetic wave of frequency almost equal to the downshifted frequency of the signal wave. The wiggler length and period look shorter by a factor γ_r, due to the Fitzgerald contraction, where $\gamma_r = (1-\beta_r^2)^{-1/2}$, $\beta_r \equiv V_r/c$ and V_r is the moving frame velocity, which is chosen to satisfy $V_r < V_{0z}$ so that $V_r - V_{0z} \ll c$. The ponderomotive axial field is the same in the moving and laboratory frames. Its wavelength is half the optical and wiggler wavelength. Hence a $\lambda_w = 2$ cm FEL experiment with $\gamma_{0z} = 100$ looks like a nonrelativistic stimulated Compton experiment with $\lambda'_w \simeq \lambda'_s = 200\ \mu$m.

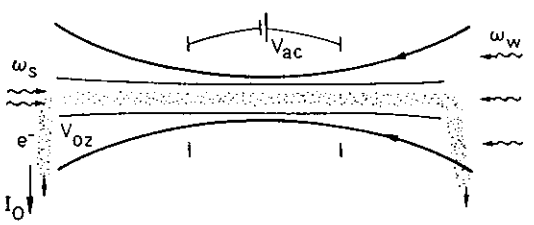

Fig. 1. The experimental scheme.

Furthermore, if we consider the case of an FEL with a tapered wiggler and our moving frame keeps moving with a velocity close to the decelerating velocity of the ponderomotive force, then the moving frame is no longer inertial. Its deceleration manifests itself by the generation of an imaginary force, which tends to accelerate the electrons in the axial direction. Thus, a tapered wiggler FEL experiment can be simulated by a Compton scattering experiment with

$$eE'_{ac} = -\frac{d}{dt'}(\gamma_r m v_r). \tag{2}$$

A FEL experiment with axial electric field can be simulated by a stimulated Compton scattering experiment with the same electric field.

Our analysis of the FEL interaction in the trapping regime is done in the relativistic frame of the ponderomotive wave [7]. In this frame the potential field is a series of static potential wells, and the force field is conservative. The concept of trap depth and axial field detrapping effects are most transparent in this frame and are displayed in fig. 2.

The electron equation of motion in the moving frame can be straightforwardly integrated and can be used to derive electron trapping conditions.

$$\frac{d}{dt'}P'_z = -eE'_{pm}\cos(k'z') - eE'_{ac}, \tag{3}$$

$$\frac{P'^2_z}{2\gamma'_m} - e\frac{E'_{pm}}{k'}\sin(k'z') + eE'_{ac}(z'-z_1) = \text{const}, \tag{4}$$

where $k' = k'_w + k'_s = 2k'_w$.

The electron trapping conditions relate to the beam energy spread $\Delta E'$, the applied axial electric field E'_{ac} (which tends to diminish the potential wells), and the space charge field effect. These conditions can be easily written in the moving frame and then transformed to the lab frame [7]:

wave frame:

$$\Delta E' = \frac{P'^2_z}{2\gamma'_m} < E'_{trap} = 2e\frac{E'_{pm}}{k'}, \tag{5}$$

$$E'_{ac} \ll E'_{pm}, \tag{6}$$

$$E'_{sc} = \frac{en'_{trap}}{\epsilon_0 k'} \ll E'_{pm}; \tag{7}$$

lab frame:

$$\Delta E < \frac{4\beta\gamma ce(\mu_0/\epsilon_0)^{1/4}(S_w S_z)^{1/4}}{(\omega_w\omega_s)^{1/2}}, \tag{8}$$

$$E_{ac} \ll E_{pm} = \frac{e}{\gamma mc^2}\frac{\lambda_w+\lambda_s}{2\pi}\left(\frac{\mu_0}{E_0}\right)^{1/2}(S_w S_s)^{1/2}, \tag{9}$$

$$E_{sc} = \left(\frac{\mu_0}{\epsilon_0}\right)^{1/2}\frac{2\gamma J_{trap}}{\beta(k_s+k_w)} \ll E_{pm}. \tag{10}$$

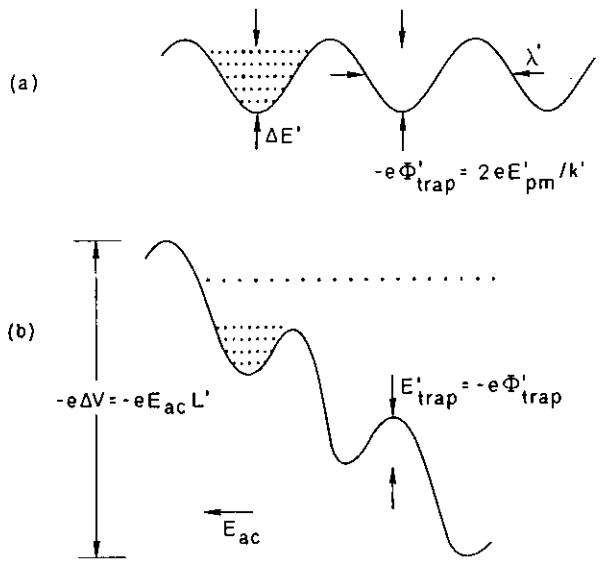

Fig. 2. The ponderomotive potential: (a) $E_{ac} = 0$, (b) $E_{ac} \neq 0$.

In our experimental set-up design we assumed: $\lambda_w = 10.8\ \mu m$, $\lambda_s = 9.2\ \mu m$, $\beta = 0.08$ ($E = 1.6$ keV), $P_w = P_s = \pi W_0^2 S_{w,s} = 10$ MW, $\pi W_0^2 = 0.1$ cm^2, $L = 50$ cm $\ll 2z_r = 200$ cm. Under these conditions, a ponderomotive field of 12.7 V/cm is calculated. If this field would be applied along 50 cm, a 635 V accelerating potential would be generated. This, however, will completely detrap the electrons. However, an accelerating voltage of 100–300 V will provide a significant enough effect on the electron energy distribution without detrapping the electrons. The calculated trap depth is 5 eV and this is a quite convenient energy spread acceptance parameter. The space charge condition (10) is easily satisfied for any practical current densities we may use. We also calculated the number of synchrotron oscillations which the nearly synchronous electrons are expected to execute around the potential well bottom within the electron transit time. The calculated number $n_{synch} = 76$ indicates that the experiment may permit detailed studies of the trapped electron phase space dynamics.

3. Experiment description

The experimental concept is illustrated in fig. 3. An electron beam is coaligned with two counter-propagating pulsed CO_2 laser beams. The wiggler is a laser beam operating a wavelength of $\lambda_w = 10.6\ \mu m$. The signal is a laser beam operating at $\lambda_s = 9.3\ \mu m$. The optical beams produce a ponderomotive potential with amplitudes given by [24] $E_{pond} = e(k_w + k_s)(A_w^* \cdot A_s)/2\gamma m$ and propagates at a velocity $V_p = C(\lambda_w - \lambda_s)/(\lambda_w + \lambda_s)$.

The electron beam is accelerated such that the elec-

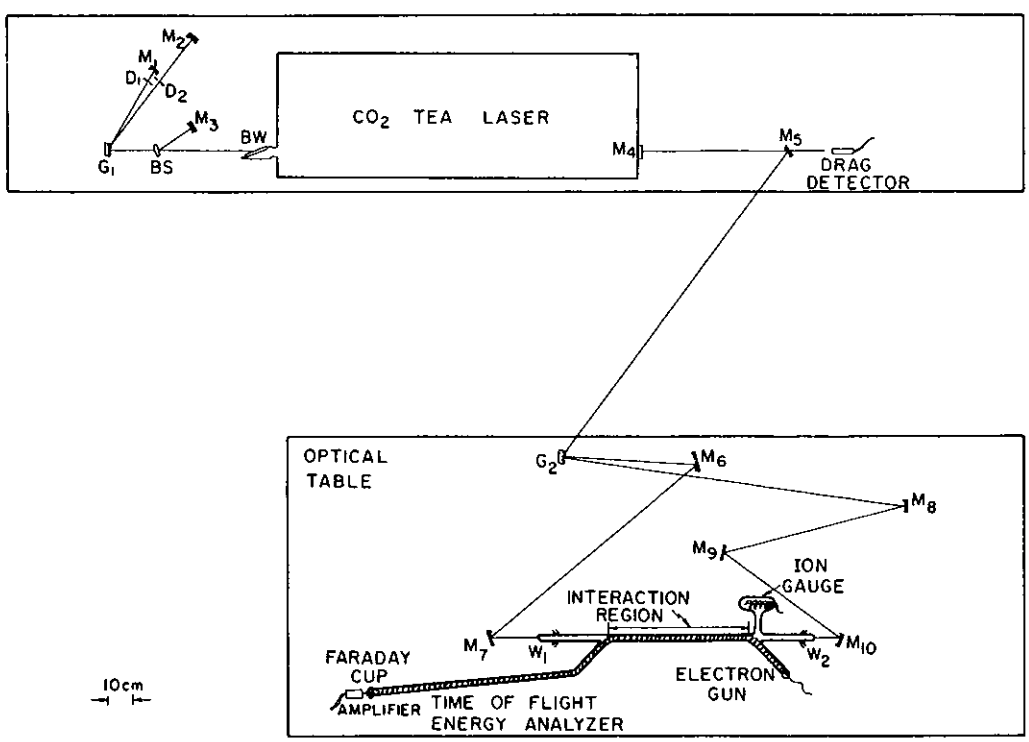

Fig. 3. General experimental setup.

trons arrive at the interaction region, i.e. the length which the laser beams interact with the electron beam, with a velocity equal to v_p. In the moving frame of the electrons there will be a static sinusoidal potential field as illustrated in fig. 2a. If an axial electric field is applied along the interaction region the potential field will appear as in fig. 2b. The additional field would normally accelerate the electrons however, the electrons within the ponderomotive potential wells would be trapped, and hence would approximately maintain their initial velocity. Upon exiting the interaction region it will be possible to determine the degree of trapping by measuring the energy distribution with an energy analyser, which is based on a time of flight scheme.

4. Laser and optics systems

The CO_2 TEA laser is configured in a manner to provide two simultaneous laser pulses at two different wavelengths, 10.6 μm and 9.3 μm. Each beam is required to be in the fundamental Gaussian transverse mode TEM_{00}. The laser is also required to operate with a single longitudinal mode. A scheme devised to accomplish these requirements which utilizes a single CO_2 TEA laser source for both wavelengths is depicted in fig. 3. It has the advantage of solving the timing problem between the pulses at the two wavelengths, since the delay between the electric discharge and the two pulses can be controlled by adjusting the lateral position of the two beams or by inserting independently losses in the paths of the beams inside the cavity. A relative disadvantage of this scheme is the reduction in power in the two beams as compared to the case when the two independent sources are present. This is due to unavoidable competition effects found when two laser transitions share the same upper vibrational level. Single longitudinal mode operation is obtained here by means of double cavities formed for each one of the laser lines. The fact that four cavities are sharing the same gain medium does require, however, precise alignment control.

The dual wavelength operation is achieved with the use of a blazed grating. Two mirrors (M_1 and M_2), each with a radius of 10 m are set at appropriate angles with respect to the grating (G_1) to obtain lasing at approximately 10.6 μm and 9.3 μm, respectively. The diaphragms (D_1 and D_2) force the laser beams to operate in the fundamental transverse mode TEM_{00}.

Single longitudinal mode operation at each wavelength is accomplished with a double cavity scheme. When two longitudinal modes from two cavities of different lengths are coincident, they will create an overall mode of high Q factor, and hence win out over other competing modes. The laser will thus operate with a single longitudinal mode. In the present scheme, the second cavity for both wavelengths is accomplished with a beam splitter (B_5) and another 10 m radius mirror (M_3).

The resultant laser beams emit the laser at the partially reflecting flat mirror (M_4). 95% of the beams are then reflected by an AR (antireflection) coated mirror (M_5), and 5% of the beams are used for monitoring the beam temporal characteristics. The beams are spatially separated with the aid of another grating (G_2). Each beam is then demagnified by about a factor of 3 to a diameter of approximately 3 mm by means of two spherical mirrors arranged as an inverted Galilean telescope (M_6 and M_7 at 10.6 μm and M_8 and M_{10} at 9.3 μm). The telescopes are also used to align the laser beams with the electron beam. The beams are directed through ZnSe AR coated windows (W_1 and W_2).

We mention finally that, in parallel, we have completed the building of a second cw CO_2 laser for the use as an injection source, so that, if required, we can operate two TEA lasers in an injection scheme.

5. Electron beam system

The general layout of the electron beam system and controls is shown in figs. 4, 5 and 6. A basic component of the system is the copper wire spiral which is inserted in the vacuum tube and encloses the electron beam. An extremely confined beam was obtained by means of the magnetic field created by the spiral. The electron gun is mounted on a ball joint on one of the ends of the tube. This joint allows the independent alignment of the gun axis with respect to the magnetic field lines. The electron gun is entirely immersed inside the magnetic field. Additional steering magnets guide the beam through a series of apertures. The purpose of these apertures is to ensure an overlap region for the electron and CO_2 laser beams, where the interaction is supposed to take place. The apertures were aligned by means of a HeNe laser. The current in the coil is pulsed in order to obtain high values of confining magnetic field (1–2 kG). The current in the coil also generates a small ohmic potential drop which produces the axial acceleration field E_{ac}. Three different pulses created by the system are shown in fig. 7: the coil current pulse; the electron beam pulse and the laser pulse. The timing of these pulses is controlled by means of two delayed pulse generators. This timing is an important factor since it determines the magnetic field strength, the axial electric field strength and the background noise at the time interval in which the interaction is taking place.

Considerable efforts were spent to minimize the noise due to electromagnetic interference (EMI). The source of the EMI noise is mainly the Lumonics 102 laser in which a capacitor is charged up to 40 kV and discharged through the gas medium triggered by a spark

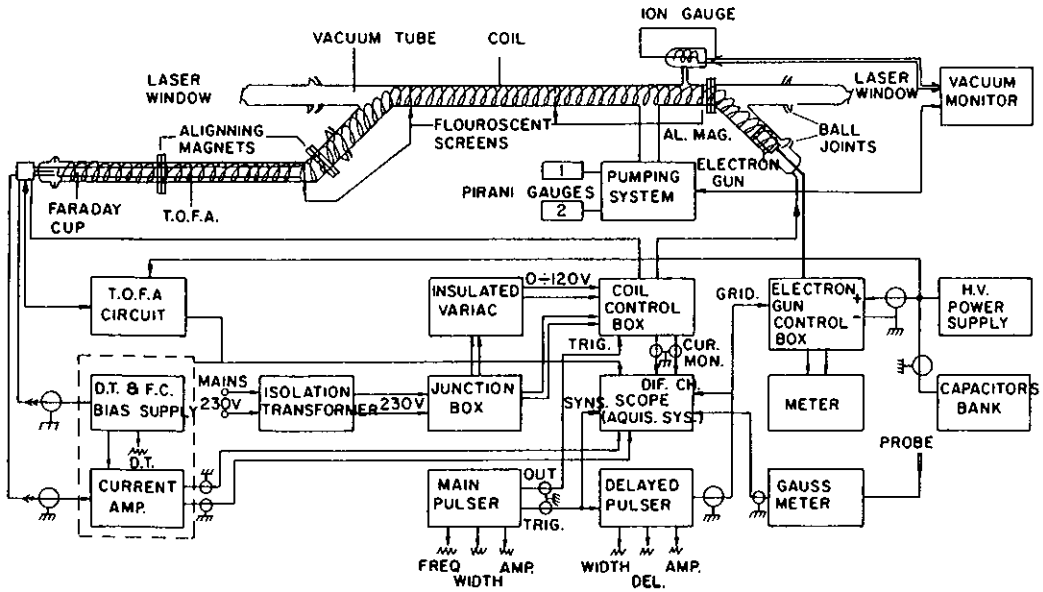

Fig. 4. Electron optical system.

gap. By means of tight shielding of the laser box, we were able to reduce the noise level by two orders of magnitude.

Figs. 8a–d are retraced oscillograms describing the electron beam current characteristics. Fig. 8a is a trace of the electron beam current incident on the walls of the time of flight drift tube. The upper trace is the current measured when the beam is optimally aligned. The lower trace is the current measured when the beam is intentionally deflected by means of an external magnet in order to hit the tube walls. It thus measures the total current in the beam (40 μA). The difference between the traces is the transmitted current. This indicates a transmission efficiency greater than 95%.

Fig. 8b represents the current measured in the Faraday cup collector. The lower trace is the current measured after the first stage of the collector amplifier. The upper trace is the current measured after the second ac coupled stage of the collector amplifier. The negative and positive spikes are proportional to the beam total current (40 μA from the width of the line trace) we conclude that the equivalent amplifier input noise current is 1 μA. This corresponds to a 2.5% trapping efficiency detection limit in our experiment.

Fig. 8c shows the effect of the laser noise on the collector amplifier signal output. The top trace is the

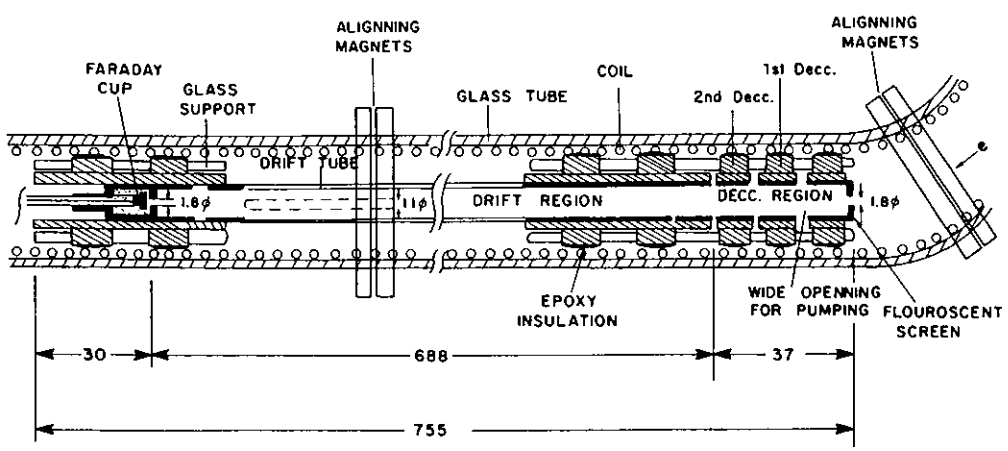

Fig. 5. "Time of flight" tube. The dimensions are in millimeters. All electrodes are made of 304 S.S.

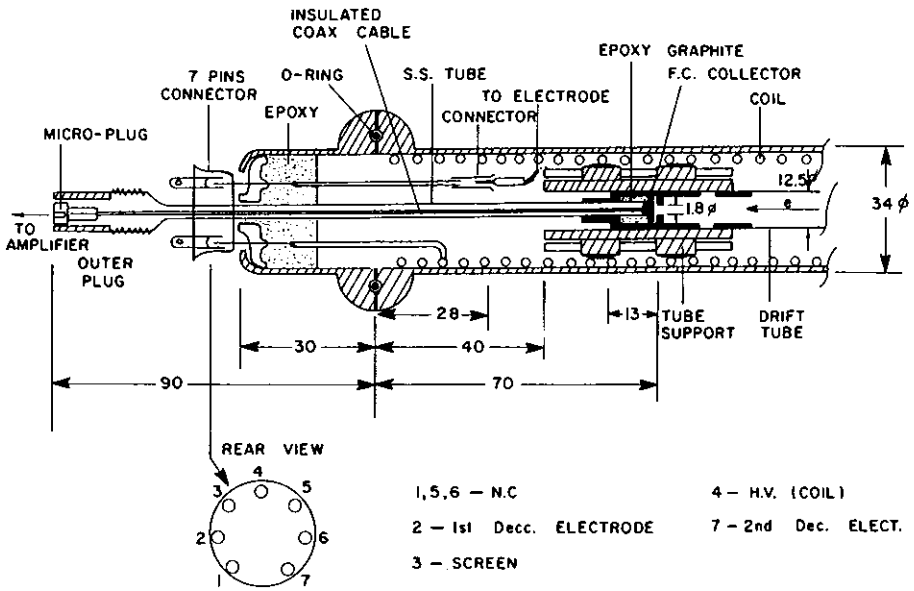

Fig. 6. Faraday cup construction and installation.

optical signal measured on the dragg detector. The center and bottom traces are the same traces as in fig. 8b but in the presence of the laser discharge EMI noise.

Fig. 8d shows the upper and medial traces of fig. 8c in a magnified scale. It is seen that in the region where the trapped electron current signal is expected (within 1 μs after the laser pulse) the EMI noise was largely eliminated, and the basic limit is given by amplifier and beam noise.

In order to estimate the signal to noise ratio in our experiment we have developed three computer programs to simulate the electron trapping effect and calculate the trapping efficiency. The first program simulates the interaction of electrons with the ponderomotive force of wiggler and signal waves. It permits also an input of more than two discrete frequencies and thus can be used to simulate the effect of multimodes in the wiggler on signal waves. This program and the simulation results are described in ref. [26].

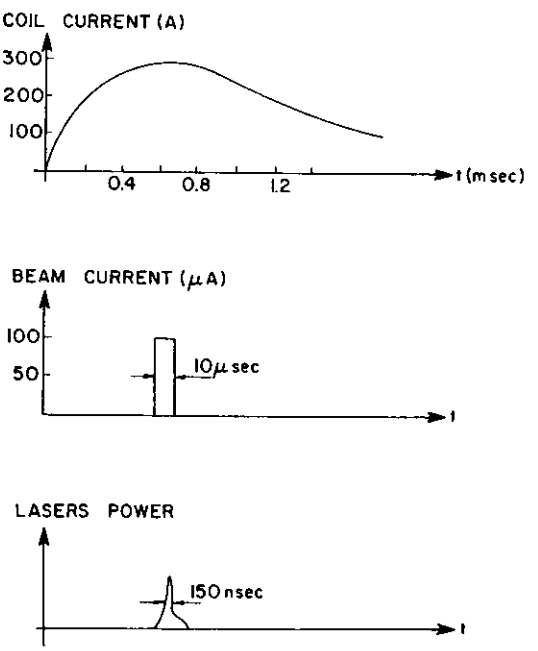

Fig. 7. Timing diagram.

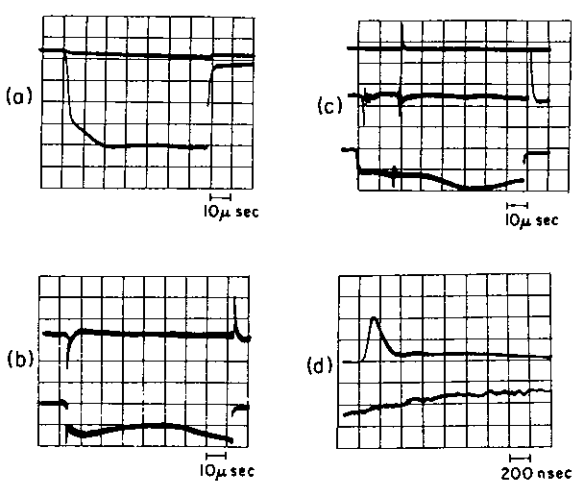

Fig. 8. Retraced oscillograms of the electron beam current.

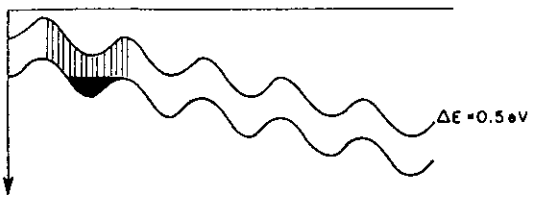

Fig. 9. Present experimental condition.

A second computer program calculates the maximum trapping efficiency in the presence of single-mode signal and wiggler waves. A typical output of the program corresponding to parameters of a recent experiment is shown in fig. 9. The parameters are shown in table 1. We do not yet have a reliable measurement of the electron energy spread and we estimate it from a retarding potential experiment to be about 10 eV. Fig. 9 indicates that the maximum trapping efficiency in the experimental conditions assumed is less than 1% which is on the border of our system detection capability.

A third program which was developed simulates the current signal which should be measured in our electron trapping experiment. It simulates the trajectories of electrons in the space–time plane along the experimental tube. The electrons are assumed to enter with random phase and given energy spread. In the interaction region their trajectories can be simulated by the second program or by other simplified model which allows shorter computation time. Figs. 12 and 13 display the computer output of this program corresponding to the

Table 1

Baseline experiment	Parameters
Signal wavelength (m)	9.33E−6
Wiggler wavelength (m)	1.07E−5
Signal power (W-peak)	6.32E+4
Wiggler power (W-peak)	1.37E+5
Electric potential (V)	1.12E+3
Beta	6.62E−2
Ponderomotive field (V/m)	6.91E+1
Ponderomotive potential (V)	5.48E−5
Max acceleration pot. (V)	4.15E+1
Trap depth w/o acc. (V)	7.01E−1
Acceleration pot. (V)	1.50E+1
Trap depth with acc. (V)	5.69E−1
Beam diameter (m)	2.00E−3
Energy spread (eV)	**Percent trapped**
0.5	29.90
1.0	7.47
1.5	3.32
2.0	1.87
2.5	1.20
3.0	0.83

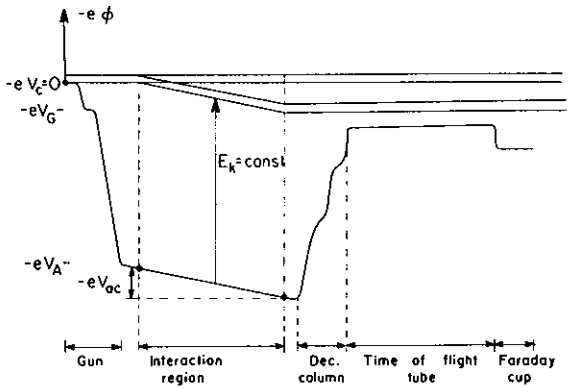

Fig. 10. Potential diagram of the tube. Acceleration in the interaction region.

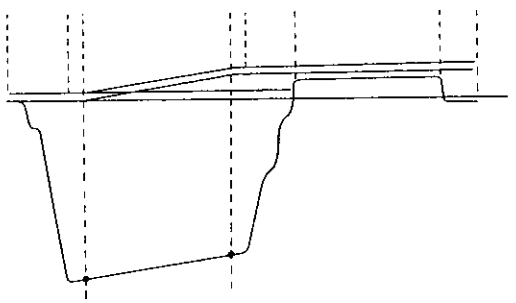

Fig. 11. Potential diagram of the tube. Deceleration in the interaction region.

physical situations depicted by the potential diagrams of figs. 10 and 11. Fig. 10 displays a situation in which an accelerating potential is applied on the electrons along the interaction region. The trapped electrons keep almost constant kinetic energy along the interaction region and emerge into the time of flight tube drift free region with lower energy than the untrapped electrons which were freely accelerated in the interaction region. Fig. 11 displays a situation in which a decelerating potential is applied across the interaction region. In the example shown the drift tube potential becomes negative relative to the cathode and all the untrapped electrons are reflected back. Only the trapped electrons, which keep constant kinetic energy within the interaction region despite the decelerating field emerge with positive kinetic energy in the time of flight tube and arrive on the collector.

Figs. 12 and 13 describe the electron trajectories and current pulse generation corresponding to the situations depicted by figs. 10 and 11 respectively. The bottom parts describe the time–space Applegate diagrams showing the trajectories of the trapped and untrapped electrons. The reflected electrons trajectories are not shown in fig. 13. The top parts show the expected

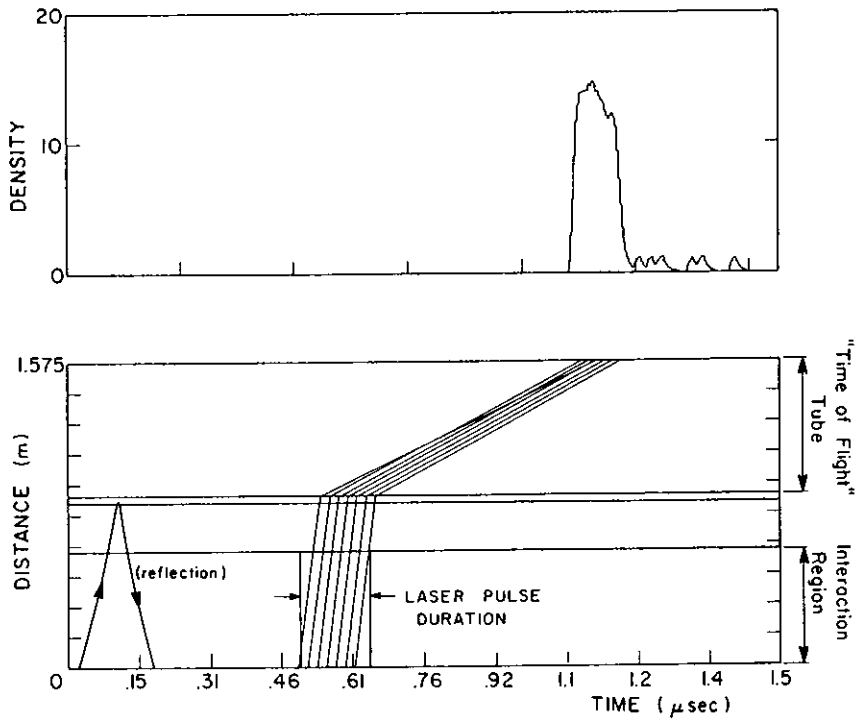

Fig. 12. Electron trajectories and current for acceleration.

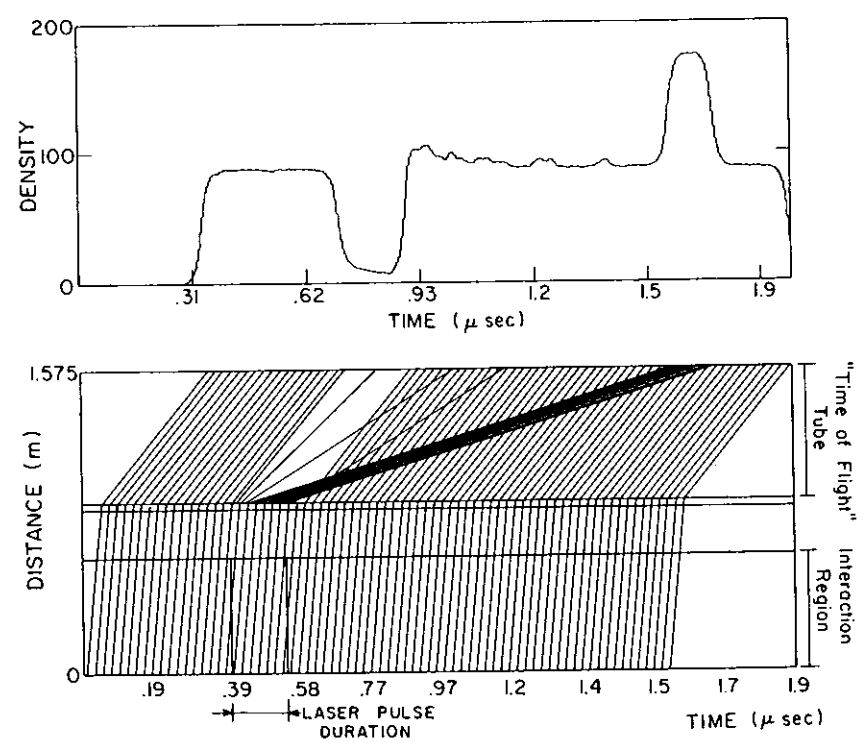

Fig. 13. Electron trajectories and current for deceleration.

current waveforms at the collector amplifier input. For simplicity the electron beam was assumed here to be completely cold and the laser powers assumed to be constant during the pulse duration. The energy spread due to the trapping effect is neglected in the present examples. Note that in the deceleration scheme (figs. 11 and 13) a single positive pulse is expected while in the other scheme an s-shaped signal is expected. We presently run the experiment in the deceleration mode where the appearance of a signal would be more easily observed.

References

[1] J.M.J. Madey, Appl. Phys. 42 (1971) 1906.
[2] D.A. Deacon, L.R. Elias, J.M.J. Madey, G.J. Ramian, H.A. Schwettman and T.I. Smith, Phys. Rev. Lett. 38 (1977) 892.
[3] R.H. Pantell, G. Soncini and H.E. Puthoff, IEEE J. Quantum Electron. QE-4 (1968) 905.
[4] V.P. Sukhatme and P.W. Wolff, J. Appl. Phys. 44 (1973) 2331.
[5] P. Sprangle and A.T. Drobot, J. Appl. Phys. 50 (1979) 2652.
[6] L.R. Elias, W. Fairbank, J. Madey, H.A. Schwettman and T. Smith, Phys. Rev. Lett. 33 (1976) 717.
[7] F.A. Hopf, P. Meystre, M.O. Sully and W.H. Louisell, Opt. Commun. 18 (1976) 413.
[8] N.M. Kroll and W.A. McMullin, Phys. Rev. A17 (1978) 300.
[9] W.B. Colson, Physics of Quantum Electronics, vol. 5, eds., S. Jacobs, M. Sargent III and M. Scully (Addison-Wesley, New York, 1978) p. 157.
[10] T. Kwan, J.M. Dawson and A.T. Lin, Phys. Fluids 20 (1977) 581.
[11] A. Hasegawa, Bell Syst. Tech. J. 57 (1978) 3069.
[12] A. Bambini, A. Renieri and S. Stehnolm, Phys. Rev. A19 (1979) 2013.
[13] I. Bernstein and J.L. Hirshfield, Phys. Rev. A20 (1979) 1661.
[14] P. Sprangle and R. Smith, Phys. Rev. A21 (1980) 293.
[15] P. Sprangle, C.M. Tang and W.M. Manheimer, Phys. Rev. A12 (1980) 302.
[16] N.M. Kroll, P.L. Morton and N.M. Rosenbluth, Physics of Quantum Electronics, vol. 7, eds., S. Jacobs, H. Piloff, M. Sargent III and M. Scully (Addison-Wesley, New York, 1980).
[17] N.M. Kroll, P.L. Morton and M.N. Rosenbluth, ibid.
[18] P. Sprangle, L.M. Tang and W.M. Manheimer, ibid.
[19] D. Prosnitz, A. Szoke and V.K. Neil, ibid.
[20] S.A. Mani, ibid.
[21] W.H. Louisell, C.D. Cantrell and W. Wagner, ibid.
[22] C.A. Bran and R.K. Cooper, ibid.
[23] J.M. Slater, J. Adamski, R.E. Center, T.L. Churchill and S.E. Moody, 11th Int. Quantum Electronics Congress (June, 1980) Digest of Papers 621.
[24] A. Gover, C.M. Tang and P. Sprangle, J. Appl. Phys. 52 (1982).
[25] A.L. Eichenbaum, US Patent 3020439 (Feb. 6, 1962).
[26] S. Ruschin, A. Friedman and A. Gover, to be published in J. Quantum Electron.